Published in final edited form as:
J Phys Chem A. 2011 November 17; 115(45): . doi:10.1021/jp204278k.

Analysis of hydrogen-bond interaction potentials from the electron density: Integration of NCI regions

Julia Contreras-García, **Weitao Yang**[*], and
Department of Chemistry, Duke University, Durham, North Carolina, 27708

Erin R. Johnson[‡]
School of Natural Sciences, University of California, Merced, 5200 North Lake Road, Merced, California, 95343

Abstract

Hydrogen bonds are of crucial relevance to many problems in chemistry biology and materials science. The recently-developed NCI (Non-Covalent Interactions) index enables real-space visualization of both attractive (van der Waals and hydrogen-bonding) and repulsive (steric) interactions based on properties of the electron density It is thus an optimal index to describe the interplay of stabilizing and de-stabilizing contributions that determine stable minima on hydrogen-bonding potential-energy surfaces (PESs). In the framework of density-functional theory energetics are completely determined by the electron density Consequently NCI will be shown to allow quantitative treatment of hydrogen-bond energetics. The evolution of NCI regions along a PES follows a well-behaved pattern which, upon integration of the electron density is capable of mimicking conventional hydrogen-bond interatomic potentials.

I. Introduction

Hydrogen bonds (HBs) play a crucial role in chemical reactivity, solvation, and materials self-assembly.[1–3] They are also fundamental in determining biomolecular structure, upon which biological function is ultimately dependent. Thus, the ability to understand and predict formation of hydrogen bonds is of great relevance to a diversity of problems in science.

The description of hydrogen bonds is still evolving[4,5] and a more inclusive definition has been recently proposed by the IUPAC.[6,7] However, the general viewpoint remains very close to the definition already proposed more than a century ago.[8–10] A hydrogen bond is understood as the attractive interaction involving an electronegative proton donor and an electronegative proton acceptor.

Semiempirical models have been developed to correlate hydrogen bond strength with geometrical parameters, such as the model of Lippincott and Schroeder.[11,12] However, such relations are usually fulfilled only for structurally-related compounds. For example, a wealth of investigations have been devoted to analyzing the relationship between the geometries of O-H···O dimers and their binding energies.[13,14]

[*]weitao.yang@duke.edu
[‡]ejohnson29@ucmerced.edu

Supporting Information Available: Binding energy curves computed at the MP2/Aug-cc-PVTZ level for all the dimers in Figure 6 are available. A plot comparing computed $s(\rho)$ values with results using STO model densities is also provided. These materials can be downloaded free of charge via the Internet at http://pubs.acs.org.

More elaborate connections between energetics and structure can be derived from the electronic density. The theory of Atoms In Molecules (AIM), pioneered by Bader and collaborators is a valuable tool for understanding hydrogen bonding in both inter- and intramolecular complexes.[15–18] This theory is able to partition a molecule into its constituent atoms by defining interatomic surfaces, such that the gradient of the density is parallel to the surface. Since a density maximum (actually a cusp) is associated with each nuclear position, the resulting partitioning bears a (nearly general)[19] one-to-one correspondence with the chemical structure. Since the atomic partition is exclusive and spans the entire space, density-based properties can be summed over the atomic regions to give molecular values. Molecular information can also be extracted from analysis of critical points of the density-gradient field. First-order saddle points can be associated with virial paths, and therefore can be used to identify the existence of chemical bonds (these points are thus called bond critical points, BCPs).[15,20] The properties of the density field, such as the density itself or its Laplacian, at the BCP can be associated with the strength of the corresponding interaction.[16,18]

The density at hydrogen-bonding critical points (HBCPs) can be related to the binding energy[16] even for unconventional hydrogen bonds, such as dihydrogen bonds.[21] However, comparisons can only be rigorously made when the nuclei participating in the bond are the same or, for semi-quantitative analysis, when they are chemically related (e.g. along a chemical series). Another problem is that density values at HBCPs cannot be used to identify the most stable geometry of a complex. As a hydrogen bond is stretched, the density at the critical point diminishes exponentially, which does not mimic the binding potential. Even more complications arise at the other end of the binding curve, when the intermolecular separation is compressed. As the two hydrogen-bonded atoms come closer, the overlap increases in a continuous manner and so does the density at the HBCP. The repulsive wall has no net effect on the density at the HBCP.

In this article, the recently-introduced Non-Covalent Interactions (NCI) index,[22,23] its derivation, and relationship to energetics, will be summarized. NCI shares many similarities with the Atoms in Molecules approach, but additionally provides three-dimensional regions around BCPs. It will be shown that NCI regions are able to model hydrogen-bonding potential-energy surfaces (PESs). The volumes and density values of NCI regions increase as the monomers come together from infinite separation, revealing a gradual transition from weak dispersive interactions at long range to hydrogen bonding in the vicinity of the minimum. At shorter separations, NCI points with positive second eigenvalue characterize the appearance of the repulsive wall. A unique definition of the NCI region will be proposed and density integration of attractive and repulsive interactions within it will be related to several conventional hydrogen-bonding PESs.

II. Theoretical Background

A. The reduced density gradient

There is ongoing interest in reconciling the traditional Lewis model of chemical bonding with the outcome of first-principles quantum-mechanical methodologies.[15,24] Quantitative and rigorous formalisms based on topological and visual analysis of scalar fields related to the electron density, $\rho(\vec{r})$, have been quite successful in this respect.

We have recently developed an index for analysis of Non-Covalent Interactions (NCI), derived from the electron density and its gradient, which enables interaction identification in real space.[22] Although mainly applied to non-covalent interactions, it can also be used to detect covalent bonds (see Supporting Information in Ref. 22).

The origin of NCI can be traced to the generalized gradient contribution to the GGA exchange energy, E_X^{GGA}, from density-functional theory:

$$E_X^{GGA} - E_X^{LDA} = -\sum \int F(s)\rho^{4/3}(\vec{r})d\vec{r}, \quad (1)$$

where $F(s)$ is a function of the reduced density gradient, s, for a given spin. The reduced density gradient accounts for local density inhomogeneities:

$$s = \frac{1}{C_F}\frac{|\nabla\rho|}{\rho^{4/3}}; \quad (2)$$

where $c_F = 2(3\pi^2)^{1/3}$ is a constant and the 4/3 exponent of the density ensures that s is a dimensionless quantity.

The reduced density gradient assumes large values in the exponentially-decaying density tails far from the nuclei, where the density denominator approaches zero more rapidly than the gradient numerator. Small values of s occur close to the nuclei, due to the combination of large densities and small density gradients, if Gaussian basis sets are used. The lower bound on the reduced density gradient is zero, as occurs throughout a homogeneous electron gas and in chemical bonds (*vide infra*).

The effect of bonding on the reduced density gradient is especially easy to visualize when s is plotted as a function of the density. Graphs of $s(\rho)$ assume the form $f(x) = ax^{-1/3}$, where a is a constant (see Fig. 1 in Supporting Information). This can be easily proved from a STO model density. For a single atomic orbital $\psi = e^{-ar}$, the density is $\rho = e^{-2ar}$ and gradient is $\nabla\rho = -2a\rho$, such that

$$s(\rho) = \frac{1}{C_F}\frac{2\alpha\rho}{\rho^{4/3}} = \frac{2\alpha}{C_F}\rho^{-1/3}. \quad (3)$$

When there is overlap between atomic orbitals, a trough in the $s(\rho)$ diagram appears. The points forming this trough can identify the interaction when they are mapped back to real space. This procedure is able to reveal non-covalent interactions, such as hydrogen bonds, steric repulsion, van der Waals interactions, and even covalent bonding.[22,23]

This approach has the advantage of being generally transferable to diverse chemical systems. The $s(\rho)$ features are very stable with respect to the calculation method, to such an extent that they are already contained in the sum of atomic densities (*aka* the promolecular density).[25] Since promolecular densities lack the relaxation introduced in self-consistent Hartree-Fock or DFT calculations, they are very fast to compute. Thus, qualitative NCI analysis is applicable to extremely large systems, including proteins and DNA, where describing the interplay of attractive and repulsive interactions is crucial for understanding functionality.[26]

B. Differentiating interactions

Further analysis of NCI peaks is needed to differentiate between interaction types. According to the divergence theorem,[27] the sign of the Laplacian of the density ($\nabla^2\rho$) indicates whether the net gradient flux is entering ($\nabla^2\rho < 0$) or leaving ($\nabla^2\rho > 0$) an infinitesimal volume around a reference point. Hence, it highlights whether the density is concentrated or depleted at that point, relative to the surrounding environment. To

differentiate between different types of weak interactions one cannot resort to the sign of the Laplacian itself (as is common within AIM theory) since it is dominated by the principle axis of variation and is positive for all closed-shell interactions.[28]

Van der Waals interactions and hydrogen bonds can be differentiated by densities at the corresponding bond critical point. Characteristic densities of van der Waals interactions are much smaller than densities at which hydrogen bonds appear. However, steric clashes and hydrogen bonds span similar density ranges and overlap in plots of $s(\rho)$. To distinguish between attractive and repulsive interactions, one must consider accumulation or depletion of density in the plane perpendicular to the interaction. This is mainly characterized by the second eigenvalue, λ_2, of the electron-density Hessian (second derivative) matrix.

In molecules, the third Hessian eigenvalue, λ_3, represents variation along the internuclear direction and is the dominant contribution to the Laplacian, whereas λ_1 and λ_2 represent variation in the plane normal to the λ_3 eigenvector. At points with zero gradient, analysis of the Hessian eigenvalues is analogous to determining the signature of a BCP.

Both van der Waals interactions and hydrogen bonds show negatives value of λ_2 at the critical point (with $\lambda_2 \leq 0$ for van der Waals interactions). This can be attributed to the homomorphic virial path associated with the bonding direction, which defines a line along which the potential-energy density is maximally negative. Conversely, non-bonding interactions, such as steric crowding, result in density depletion, such that $\lambda_2 > 0$. Analogously, the homeomophism ensures that these critical points (both ring and cage points) identify lines of minimally-negative potential-energy density.

Thus, the interaction type can be distinguished if the $s(\rho)$ diagrams are modified by plotting $\text{sign}(\lambda_2)\rho$ as the ordinate. This is illustrated for the example of phenol dimer in Figure 1. This is a hydrogen-bonded complex that also exhibits non-bonding interactions within each benzene ring at overlapping density ranges. When the Hessian eigenvalues are considered, the different nature of these interactions is made clear: the benzene-ring interactions remain at positive values, whereas the hydrogen bond now lies at negative values, within the attractive regime. The NCI troughs nearest zero density correspond to weakly-attractive dispersion interactions between the phenyl rings.

C. Relationship to AIM

The existence of a BCP in a chemical system has a direct consequence on the $s(\rho)$ diagram. At the critical points, $s = 0$ due to annihilation of the density gradient. In regions immediately surrounding the critical point, the change in $\nabla\rho$ dominates and $s(\rho)$ approaches zero, giving rise to a steep trough. Thus, NCI agrees with the Atoms In Molecules approach in characterization of interatomic interactions.

NCI representation is able to reveal not only the topological features of the density, but their effects in real space as well, by providing chemically-intuitive isosurfaces. Figure 2a shows a $s = 0.6$ au NCI isosurface for formic acid dimer. AIM critical points have also been included in order to show the relationship between the two approaches. Isosurfaces appear around each non-covalent critical point: two isosurfaces for the symmetric hydrogen bonds associated with (3, −1) BCPs and one associated with the (3, +1) ring point at very low density. In this complex the critical points correspond to separate NCI surfaces, but this is not always the case. Figure 2b shows the $s = 0.6$ au isosurface for benzene dimer, again with its density critical points. In this case (3, −1), (3, +1), and (3, +3) critical points are extremely interrelated and embedded into the same NCI isosurface. The NCI isosurface has chemical meaning as a whole superbasin that highlights the van der Waals interaction between monomers.[29]

NCI is able to recover the features of AIM in real space, but NCI features are present even in the absence of density critical points. Figure 3a shows the $s(\rho)$ diagram for the neopentane molecule, $C(CH_3)_4$. A deviation from the $\rho^{-1/3}$ decay appears at low density and low s, on the positive side of the diagram (i.e. the non-bonding regime). In real space, the points giving rise to this peak appear between the methyl groups and appear to correspond to regions of steric hindrance. However, the peak does not reach $s = 0$, which means that no critical point is associated with this interaction. AIM topology is blind to this steric hindrance.

III. Stretching Hydrogen Bonded Dimers

Potential-energy curves of hydrogen-bonded complexes result from the interplay of attractive and repulsive contributions, which should ultimately originate from changes in the electron density.[30] However, quantitatively tracing the binding energy back to the density changes in real space is still an unsolved issue. Given that NCI is able to characterize both favorable and unfavorable interactions in real space, it exhibits all the ingredients needed to identify the changes in electron density which give rise to molecular stabilization. Moreover, the ability of NCI to associate real-space regions with non-covalent interactions enables analysis of properties within these regions, which are subject to change in a quantifiable manner upon stretching.

A. Changes in density and gradient

Figure 4 shows $s(\rho)$ diagrams and NCI isosurfaces for selected points on the water dimer potential energy surface. At very long separations (> 3.5Å), the NCI region reduces to the BCP: the $s(\rho)$ peak is extremely sharp, such that the NCI surface and critical point basically coincide. The stabilization of the complex hardly extends to other regions of space beyond the critical point itself. As we will see, the volume of the NCI region can be associated with the degree of stabilization. Thus, at infinite separation, NCI is able to supersede the symmetry constraints that compel the appearance of a critical point and identify that the monomers are not interacting at infinite separation.

As the two water molecules begin to approach and interact, the area of the $s(\rho)$ trough increases, which translates to a more voluminous NCI region. The low density at the iso-surface (and at the critical point) identify the interaction as dispersive in nature. In Figure 4 the van der Waals interaction is characterized by the green color at the isosurface.

As the water molecules continue to approach, the NCI region becomes larger in volume and bluer in color. This can be understood as the process of hydrogen bond formation. From the $s(\rho)$ diagram, it can also be cast as an increase the area of the trough. The shape changes from a sharp spike, which we have associated with van der Waals interactions, to hydrogen bonding, where the interaction spreads over more of the diagram (i.e. over a broader intermolecular space).

Upon further compression, intermonomer repulsion begins to appear. This can be seen on the positive side of the $s(\rho)$ diagram as a deformation from the expected $s(\rho) = a\rho^{-1/3}$ behavior. This deviation is reflected in the 3D plots as a red ring surrounding the attractive NCI piece (see Fig. 4e). The ability of NCI to identify the repulsive wall of intermolecular interactions goes beyond analysis of AIM graphs, since this region is not associated with any critical point. It reflects the deformation of densities in a more subtle manner that does not give rise to a change in the region of stability, according to the catastrophe theory of Thom within the AIM framework.[31]

NCI provides rich information beyond common, local analysis of critical points. It is able to identify interactions occurring along the entire potential-energy curve of a hydrogen-bonded complex: progressing from no interaction at infinite separation, to weak van der Waals attraction, hydrogen-bond formation, and finally short-range repulsion. This last feature cannot be derived from mere analysis of critical points because it is related to the region surrounding the BCP, not to a BCP itself.

The existence of BCPs has been related to preferred exchange channels.[32] This picture is complemented by NCI, which predicts a favourable, binding interaction (blue) in water dimer, surrounded by an unfavourable interaction (red) giving rise to the repulsive wall. Although exchange between two monomers favors their interaction, at very short separations an unfavorable atomic-density overlap arises, which is not localized along the virial path, but around it.

B. Integration over NCI regions

Given that the volumes of the attractive and repulsive NCI regions can be visually related to various regions of the binding curve, we investigated whether integration of NCI regions permits quantitative analysis of stabilizing and destabilizing contributions along the PES. In order to perform such integrations, it is necessary to establish a unique definition of the NCI region.

Since the difference between the interacting and non-interacting monomers is directly reflected in the $s(\rho)$ diagram, it is possible to define the NCI region as the points in 3D space with (ρ,s) values lying in the $s(\rho)$ peak. To identify this region, both the monomer and the dimer densities must be computed and compared. The lower edge of the monomer $s(\rho)$ curve is splined and all points of the dimer $s(\rho)$ plot lying below the splined curve are localized in real space.

Density properties can be integrated within this space to obtain the volume (V) of the NCI region, or the charge (q) enclosed within it.

$$V_{NCI} = \int_{\Omega NCI} d\vec{r} \quad (4)$$

$$q_{NCI} = \int_{\Omega NCI} \rho(\vec{r}) d\vec{r} \quad (5)$$

In practice, these integrations are performed numerically, by summation over a cubic grid with 0.1 au increments.

Fig. 5a shows the volume of the water dimer NCI region as a function of intermonomer separation. As already observed in Fig. 4, the volume of the interacting region is negligible at very long distances. As the monomers come closer together, the volume starts to increase, with the volume of the attractive region growing faster than the repulsive one. At around $R_{O-H} = 2.5\text{Å}$ the volume of the attractive region reaches a maximum and, at shorter separations, changes in the repulsive region become the dominant contribution to the total volume. This result again highlights the necessity of considering the entire non-covalent interaction region rather than just the critical point to understand the corresponding energetics.

When the density of the NCI region is taken into account, Fig. 5b is obtained. Although the same overall behavior as Fig. 5a is maintained, the shape of the curves change due to the fact that the density in the intermolecular region increases upon dimer compression. The

attractive contribution increases more notably at shorter distances, whereas the repulsive part, where the overlap is smaller, increases more slowly. Results for the density at the critical point have been included for comparison. Both $\rho(BCP)$ and the density associated with the NCI region increase upon compression. However, the NCI density can be decomposed into an attractive ($\lambda_2 < 0$) component that dominates at long-range and a repulsive ($\lambda_2 > 0$) component that offsets, and eventually surpasses, the attractive term at short-range. This reflects the onset of the repulsive wall in the potential-energy surface. Indeed, integration of interaction regions has already been found to hold the key for problematic situations withing AIM theory. The diffuse valence electrons in organometallic compounds give rise to critical points at very low densities and whose positions are unstable with respect to methodology or geometry changes. In those cases, the electron density integrated over the whole interatomic surface provides an alternative, and more informative, index.[33]

C. Binding energy

Intermolecular potentials are a frequent subject of computational modeling and are fundamental in simulations of molecular reactivity and materials stability. The atomic potential approach, used in semiempirical description of complicated many-body processes, models the binding energy in terms of pair-wise interactions between the atoms of different molecules. The main problem associated with such potentials is that they are parameterized for common pairs of atoms in established chemical environments. Thus, they are not necessarily applicable to other bonding situations.

Taking into account the fundamental theorem that binding energies must results from changes in the electron density,[30] it would be extremely desirable to be able to formulate interatomic potentials using the real-space behavior of the density. A first step in this direction was taken by Espinosa et al.[34] who showed that binding-energy curves for O···H hydrogen bonds can be fit in terms of the potential and kinetic energy densities at the BCP.

It is our aim to expand this approach by including all points in the NCI region, already shown to exhibit a qualitative correspondence with energetics. First, the interaction region is isolated as described in Section IIIB. Then, points are identified as contributing mainly to the potential energy (attractive regime) or the kinetic energy (repulsive regime) of the system. According to the local virial theorem:

$$\frac{1}{4}(\lambda_1+\lambda_2+\lambda_3) = 2G(\vec{r}) + V(\vec{r}) \quad (6)$$

the potential energy and kinetic energy densities are interrelated by the Hessian eigenvalues at all points in space.[20] For all non-covalent interactions, the Laplacian is positive due to the dominant contribution from λ_3 along the interatomic vector. In order to understand the attractive/repulsive interplay in these systems, it is necessary to analyze the density derivatives in the plane perpendicular to the λ_3 eigenvector (across which density accumulates/depletes). Since the most important contribution in this plane is coming from λ_2, it contains the information needed to determine whether the potential or the kinetic energy density prevails at each point, or equivalently, whether the attractive or repulsive interactions dominates.

As in Fig. 5, it is convenient to separate the attractive and repulsive contributions depending on the sign of the second eigenvalue at each point:

$$q^n_{att}=\int_{\Omega(NCI)}\rho^n(\vec{r})d\vec{r} \quad | \quad \lambda_2(\vec{r})<0 \quad (7)$$

$$q^n_{rep}=\int_{\Omega(NCI)}\rho^n(\vec{r})d\vec{r} \quad | \quad \lambda_2(\vec{r})>0 \quad (8)$$

$$q^n_{bind}=-\left(q^n_{att}-q^n_{rep}\right); \quad (9)$$

where we have assumed that binding can be approximated as the difference between the attractive and repulsive contributions. The negative sign is included to account for stabilizing interactions. Different exponents, n, have been considered in order to find the relationship that best fits known binding-energy behavior.

Figure 6 shows the results for four conventional hydrogen bonds: $H_2O\cdots H_2O$, $HF\cdots HF$, $H_2O\cdots HF$ and $H_2O\cdots NH_3$. Exponents were chosen in the range of dependencies of the potential-energy and kinetic-energy densities on ρ ($\rho^{4/3}$ and $\rho^{5/3}$, respectively). The difference between both charge contributions, $-\left(q^n_{att}-q^n_{rep}\right)$, is able to mimic very reliably the binding energy curves. When the attractive/repulsive nature of these contributions is taken into account, the behavior of the binding energy curve can be well understood in real space.

Note that the unevenness of the q^n_{bind} curves (and oscillatory behaviour in the $HF\cdots HF$ case) is a consequence of integration grid choice. Similar grid dependence is seen in potential-energy surfaces for dispersion-bound complexes obtained using meta-GGA functionals.[35]

For each exponent, n, the different slopes of the attractive and repulsive portions leads to a shift in the binding curves. When comparing with MP2 or DFT reference data, the best fits are obtained for $n \in [4/3 – 5/3]$. For these exponents, the positions of the minima (one of the main characteristics of interatomic potentials) are recovered and the shapes of the curves mimic very well the shapes of the reference binding curves.

IV. Computational Details

The binding curves were produced using the Gaussian suite of programs[36] at the MP2 level. Augmented correlation consistent basis sets of Dunning (Aug-cc-pVTZ) were used to ensure a correct description of the hydrogen bond interaction at all distances. Calculations were carried out with constrained intermonomer separations, varying from 1.0-4.0 Å in 0.1 Å increments. The remaining coordinates were optimized with the Berny algorithm.[37] Details of the PESs can be found in the Supporting Information.

Plots of $s(\rho)$ were obtained from the NCIPLOT program developed by the authors.[23,38] B3LYP/6-31G* wavefunctions and grids of 0.1 au were used unless otherwise stated. Details of the software and manual may be downloaded at http://www.chem.duke.edu/~yang/software.htm.

A new version of the program was developed to perform the volume and charge integrations. It computes (non-SCF) pseudo-densities for each of the monomers and splines the resulting $s(\rho)$ curve. The resulting line is used as a reference in order to identify which $s(\rho)$ points are only present in the dimer (Fig. 5). Density properties are summed over the dimer grid points in order to compute the integrals in Eqs. 7-9.

V. Conclusions and Future Outlook

We have shown that the NCI (Non-Covalent Interactions) index can be related to the AIM (Atoms In Molecules) approach to chemical bonding. The NCI features are tied to critical points of the density gradient field. NCI isosurfaces are also able to reveal how these critical points are connected in real space, sometimes forming superbasins. This explains why ring or cage points are sometimes a better reference for understanding bond strength than bond points themselves. Moreover, NCI is able to reveal interactions that cannot be found by analysis of critical points alone, such as the steric repulsion between methyl groups in neopentane.

We have also uniquely defined interaction volumes, within which density-based integrations can be performed to obtain properties associated solely with the interacting region. Evolution of these quantities along the potential-energy surface have been shown to reproduce the interplay of attractive and repulsive interactions seen throughout hydrogen-bond formation. Integration of charges within the interacting region has been shown to mimic very closely the interatomic potentials of conventional hydrogen bonds.

Work is in progress to extend this analysis to other types of bonding, including non-conventional hydrogen bonds and complexes with multiple interactions. Ultimately, the purpose is to relate the properties of the interacting region with those of the interatomic potentials, specifically the position and depth of the binding well.

Supplementary Material

Refer to Web version on PubMed Central for supplementary material.

Acknowledgments

This work is supported by the National Science Foundation (CHE-06-16849-03 & CHE-1012357), and the National Institute of Health through the UPCMLD project (P50GM067082) and ROI-GM-061870. J.C.G. thanks the Spanish Ministry of Education for a postdoctoral grant (EDU/2253/2010) and projects CTQ2009-14596-C02-02 and MALTA-Consolider CSD2007-00045 for computational resources.

References

1. Jeffrey, GA.; Saenger, W. Hydrogen Bonding in Biological Structures. Springer; Berlin: 1991.
2. Dunitz, JD. X-ray Analysis and the Structure of Organic Molecules. Cornell University Press; Ithaca: 1979.
3. Desiraju, GR. Crystal Engineering The Design of Organic Solids. Elsevier; Amsterdam: 1989.
4. Cybulski S, Scheiner S. J Am Chem Soc. 1987; 109:4199.
5. Seiler P, Weisman GR, Glendening ED, Weinhold F, Johnson B, Dunitz JD. Angew Chem Int Ed Engl. 1987; 1175:26.
6. Desiraju GR. Angew Chem Int Ed Engl. 2011; 50:52. [PubMed: 21031379]
7. Arunan E, Desiraju GR, Klein RA, Sadlej J, Scheiner S, Alkorta I, Clary DC, Crabtree RH, Dannenberg JJ, Hobza P, Kjaergaard HG, Legon AC, Mennucci B, Nesbitt DJ. Pure Appl Chem. 2010 in press.
8. Moore TS, Winmill TF. J Chem Soc. 1912; 101:1635.
9. Pauling, L. The nature of the chemical bond. Cornell University Press; Ithaca: 1960.
10. Pimentel, GC.; McClellan, AL. The Hydrogen Bond. Freeman; San Francisco: 1960.
11. Smallwood CJ, McAllister MA. J Am Chem Soc. 1997; 119:11277.
12. Lippincott ER, Schroeder R. J Chem Phys. 1955; 23:1099.
13. Grabowski SJ. Tetrahedron. 1998; 54:10153.
14. Grabowski SJ. J Mol Struct. 2000; 552:153.

15. Bader, RFW. Atoms in Molecules: A Quantum Theory. Oxford University Press; Oxford: 1990.
16. Espinosa E, Souhassou M, Lachekar H, Lecomte C. Acta Crystallogr B. 1999; 55:563. [PubMed: 10927398]
17. Gatti C, Saunders VR, Roetti C. J Chem Phys. 1994; 101:10686.
18. Grabowski SJ. J Phys Chem A. 2001; 105:10739.
19. Martín Pendás A, Blanco MA, Costales A, Mori Sánchez P, Luaña V. Phys Rev Lett. 1999; 83:1930.
20. Bader RFW, Beddall PM. J Chem Phys. 1972; 56:3320.
21. Grabowski SJ. J Mol Struct. 2000; 553:151.
22. Johnson ER, Keinan S, Mori-Sánchez P, Contreras-García J, Cohen AJ, Yang W. J Am Chem Soc. 2010; 132:6498. [PubMed: 20394428]
23. Contreras-García J, Johnson ER, Keinan S, Chaudret R, Piquemal JP, Beratan DN, Yang W. J Chem Theory Comput. 2011; 7:625. [PubMed: 21516178]
24. Silvi B, Savin A. Nature. 1994; 371:683.
25. Spackman MA, Maslen EN. J Phys Chem. 1986; 90:2020.
26. a Fiedler S, Broecker J, Keller S. Cell Mol Life Sci. 2010; 67:1779. [PubMed: 20101433] b Dill KA. Biochemistry. 1990; 29:7133. [PubMed: 2207096]
27. Arfken, G. Mathematical Methods for Physicists. Academic Press; Orlando: 1985.
28. Bader RFW, Essén H. J Chem Phys. 1984; 80:1943.
29. Silvi B. J Mol Struct. 2002; 614:3.
30. Hohenberg P, Kohn W. Phys Rev B. 1964; 136:864.
31. Polo V, Andres J, Castillo R, Berski S, Silvi B. Chem Eur J. 2004; 10:5165. [PubMed: 15372667]
32. Martín Pendás A, Francisco E, Blanco MA, Gatti C. Chem Eur J. 2007; 13:9362. [PubMed: 17674344]
33. Macchi P, Sironi A. Coordination Chemistry Reviews. 2003:238–239. 383–412.
34. Espinosa E, Molins E. J Chem Phys. 2000; 113:5686.
35. Johnson ER, Becke AD, Sherrill CD, DiLabio GA. J Chem Phys. 2009; 131:034111. [PubMed: 19624185]
36. Frisch, MJ., et al. Gaussian 03, Revision C.02. Gaussian Inc; Wallingford: 2004.
37. Schlegel HB. J Comp Chem. 1982; 3:214.
38. http://www.chem.duke.edu/~yang/Software/softwareNCI.html

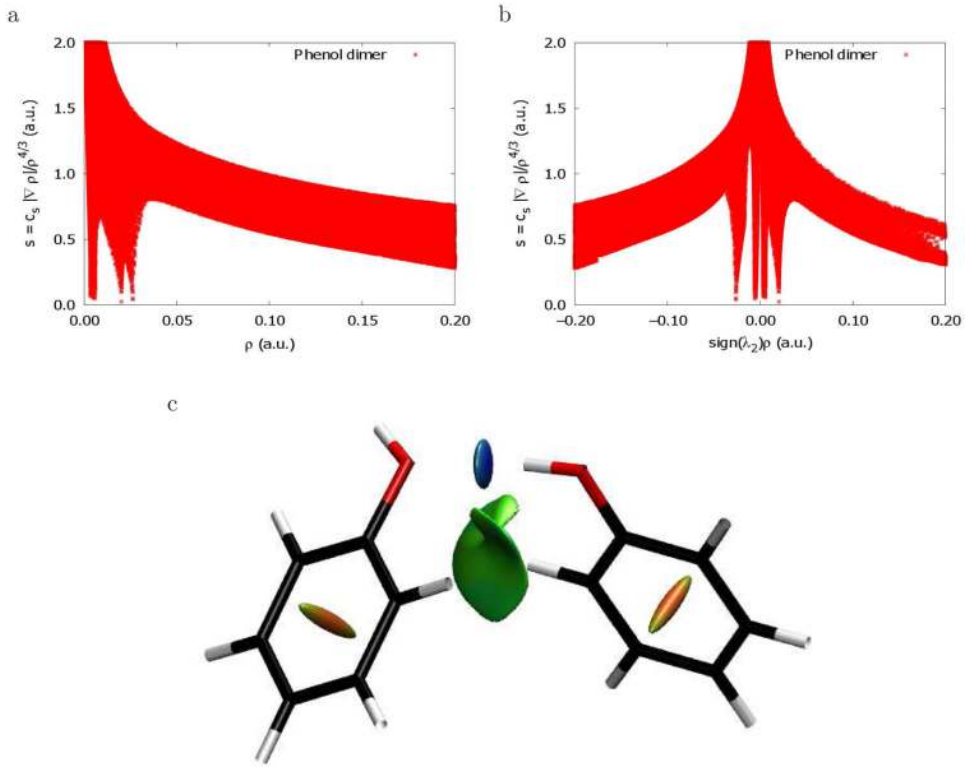

FIG. 1.

Plots of (a) $s(\rho)$, (b) $\text{sign}(\lambda_2)\rho$, and (c) NCI isosurface, for the phenol dimer. The $s = 0.6$ au isosurface is colored according to a BGR scheme over the range $-0.03 < \text{sign}(\lambda_2)\rho < 0.03$ au. Blue indicates strong attraction, green indicates very weak interaction, and red indicates strong repulsion.

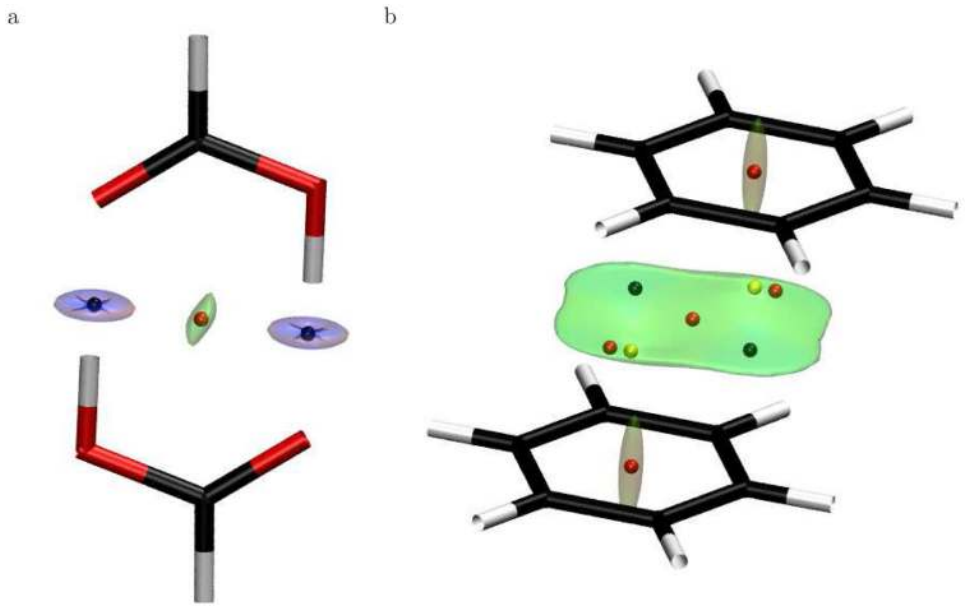

FIG. 2.

NCI isosurfaces for a) formic acid dimer and b) benzene dimer. Isosurfaces were generated for $s = 0.6$ au and $-0.4 < \text{sign}(\lambda_2)\rho < 0.4$ au. Critical points of the density have been included for comparison and are coloured according to their signature: (3, −1) = black, (3, +1) = red, and (3, +3) = yellow.

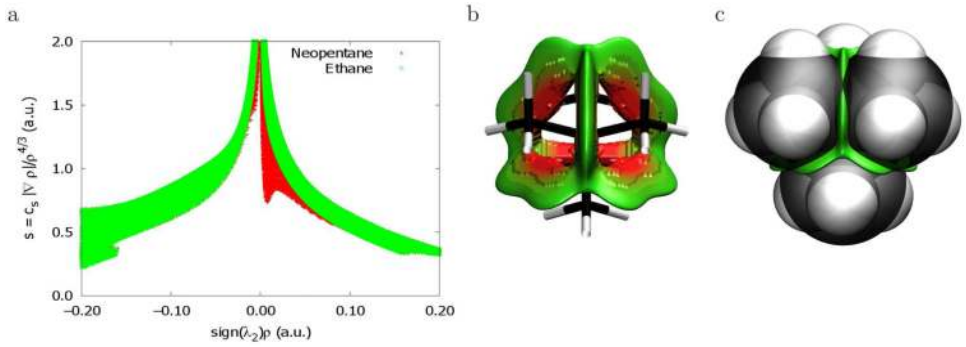

FIG. 3.

Plot of a) $s(\rho)$ and b) NCI isosurfaces for neopentane, $C(CH_3)_4$. Isosurfaces with $s = 1.2$ au were generated for the region below the lower edge of the ethane curve. A scale $-0.03 < \text{sign}(\lambda_2)\rho < 0.03$ au was used to color the isosurfaces. Van der Waals spheres have been added in (c) to highlight the steric nature of the interaction.

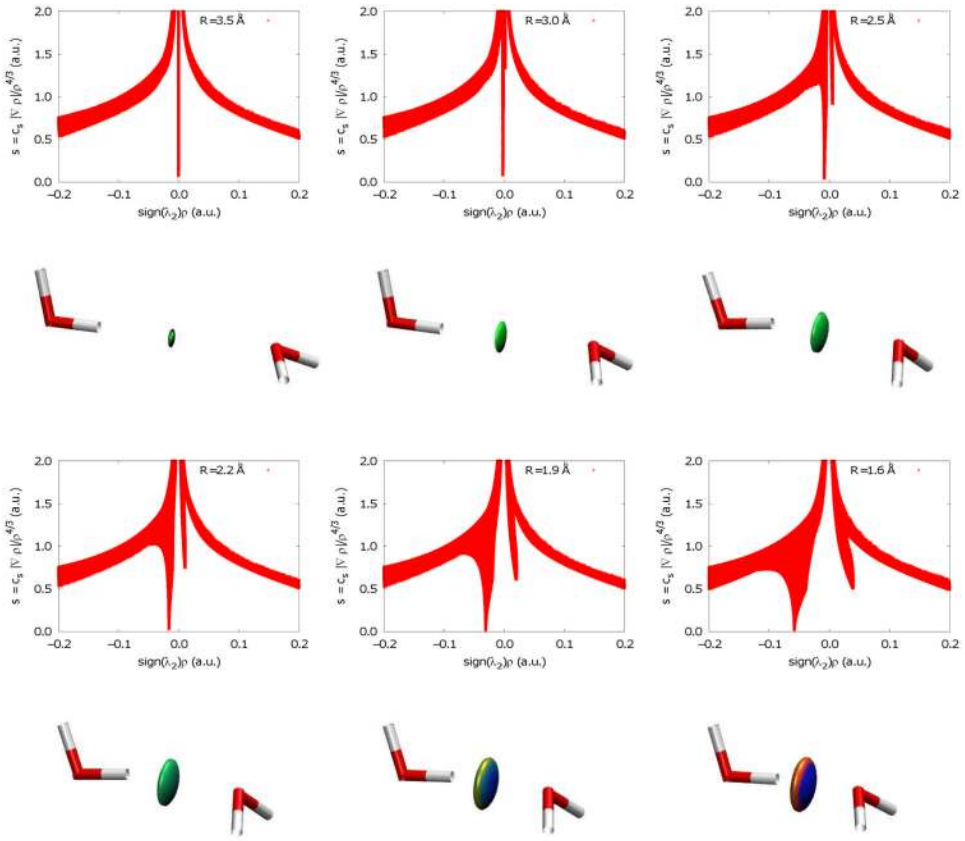

FIG. 4.

Evolution of $s(\rho)$ diagrams and NCI isosurfaces along the water dimer potential energy surface. Representative distances have been chosen to highlight the various interaction regimes: non-interacting, van der Waals attraction, hydrogen bonding, and steric repulsion. Isosurfaces were generated for $s = 0.6$ au and $-0.04 < \text{sign}(\lambda_2)\rho < 0.04$ au.

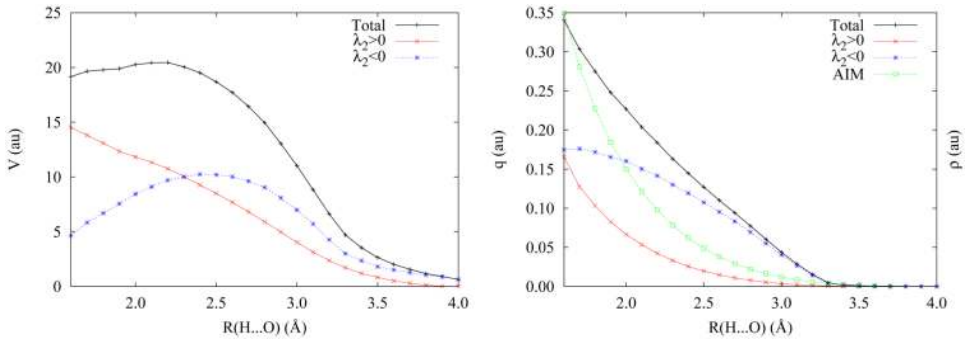

FIG. 5.

Volume (left) and charge (right) integrations within the hydrogen bond NCI region of water dimer, separated into attractive ($\lambda_2 < 0$) and repulsive ($\lambda_2 > 0$) contributions. The density at the BCP has been included for comparison in the charge integration plot (right).

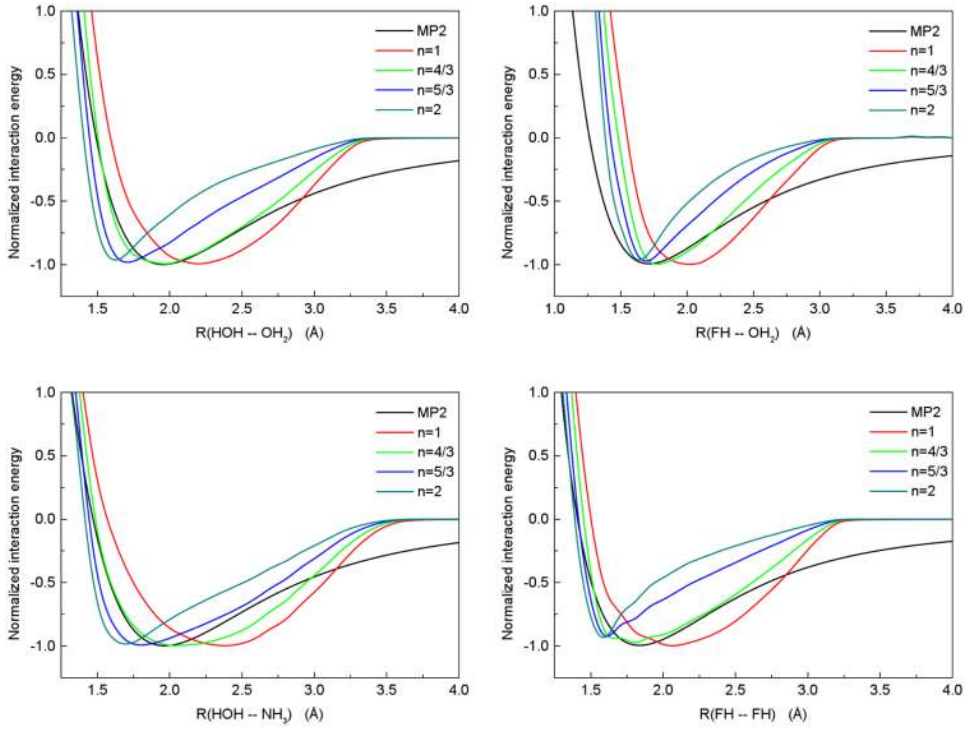

FIG. 6.

Binding energies and q^{n}_{bind} (Eq. 9) for $H_2O\cdots H_2O$, HF⋯HF, $H_2O\cdots HF$ and $H_2O\cdots NH_3$.

Results for several exponents ($n=1, \frac{4}{5}, \frac{5}{3}$ and 2) are collected for comparison. All the curves are normalized to minimum values of -1.